REAL-TIME PILOT INPUTS FOR AIRCRAFT DYNAMIC MODELING

Eugene A. Morelli[1]
NASA Langley Research Center
Hampton, Virginia, 23681, USA
e.a.morelli@nasa.gov

ABSTRACT

Real-time dynamic modeling and pilot displays are used to enable pilots to intuitively discover effective multi-axis inputs for aircraft dynamic modeling during flight tests. An F-16 nonlinear simulation flown by a pilot using a joystick and a laptop computer with real-time displays of relevant information is used to demonstrate the approach. Results show that pilots can use the real-time display to discover and implement effective and efficient multi-axis inputs for accurate dynamic modeling in flight. The real-time dynamic modeling results driving the pilot display can be used to certify that the acquired flight data are adequate for accurate dynamic modeling, thus avoiding postflight data analysis and modeling by an analyst to make that determination. Implications for pilot training and efficient flight testing are discussed.

NOMENCLATURE

α	angle of attack, rad or deg
β	sideslip angle, rad or deg
j	imaginary number = $\sqrt{-1}$
p, q, r	roll, pitch, and yaw body-axis angular rates, rad/s
$\mathrm{Re}(\cdot)$	real part of a complex number
T	maneuver length, s
$\delta_s, \delta_a, \delta_r$	stabilator, aileron, and rudder deflections, rad or deg
ω	angular frequency, rad/s

Superscripts

^{T}	transpose
$^{-1}$	matrix inverse
$\hat{}$	estimate
$\dot{}$	time derivative
†	complex conjugate transpose

[1] SFTE Member

1. INTRODUCTION

Traditionally, pilot inputs used to collect flight test data for aircraft dynamic modeling are specified prior to flight. Examples are doublets, 3-2-1-1 multisteps, and frequency sweeps [1,2]. Significant time and effort are expended to train pilots on how to properly implement these inputs, and to make sure that the inputs realized by the pilot are sufficiently similar to the ideal waveforms. Typically, the success of the pilot input implementation is determined by postflight data analysis and modeling. This is an indirect evaluation of the pilot inputs, usually done by an analyst who was not the pilot. Furthermore, these single-axis inputs can be inefficient and ineffective, particularly for stability and control flight testing in multiple axes or when control interaction effects are important. Data quality and flight test efficiency could be improved if the flying skills of the pilot were used to generate multi-axis inputs in real time.

Past flight tests using multiple simultaneous pilot inputs have used real-time cross plots of control surface deflections in flight [3] or preflight training based on input correlations and frequency content [4] to help the pilot implement inputs that produce informative data for dynamic modeling. However, these approaches used data that are not direct indicators of dynamic modeling accuracy.

Advances in real-time dynamic modeling, computer capabilities, flight instrumentation, and real-time graphics have made it possible to compute and display dynamic modeling results in real time [1,5-10]. The quality of the flight data for aircraft dynamic modeling depends strongly on the inputs applied to excite the aircraft dynamic motion, subject to the constraint that aircraft response must be kept within specified maneuver envelope limits, to ensure flight safety and the validity of an assumed model structure. Flight data quality for dynamic modeling purposes can be quantified by model parameter uncertainties computed and displayed to the pilot in real time. Consequently, the pilot can be guided toward effective and efficient multi-axis inputs by a real-time display that directly indicates the data quality for dynamic modeling. As the pilot applies inputs to excite the aircraft dynamic response to produce flight data with good information content for dynamic modeling, real-time model parameter uncertainties will be reduced.

The instruction to the pilot can be simply the following:

Maneuver to make the bars on the display (representing model parameter uncertainties) smaller than the target values shown, as quickly as possible, without exceeding the maneuver envelope limits for selected quantities (e.g., angle of attack and sideslip angle) indicated on the display.

With this approach, the pilot can use flying skills to intuitively synthesize multi-axis inputs that efficiently produce informative flight test data for dynamic modeling. This takes the analyst out of the loop by removing the need to describe input waveforms, amplitudes, and phasing to the pilot, who must then absorb that information on the ground and try to reproduce the correct inputs in flight. Instead, the creativity and flying skills of the pilot are used to directly discover effective and efficient multi-axis inputs by presenting a display of model quality metrics to the pilot in real time. Displaying real-time model metrics and target values to the pilot in flight means the pilot will know when the maneuver is complete (i.e., enough informative flight data have been collected for accurate dynamic modeling) and the testing can move on to the next flight condition or test point. This contrasts with the conventional approach of specifying the input and maneuver length on the ground, prior to the flight test, based on preflight estimates of the aircraft dynamic response

and maneuver times that will be required to achieve modeling accuracy goals. Finally, pilots will naturally and quickly learn input characteristics that are effective for each specific aircraft and flight condition, thus improving their overall effectiveness and training as test pilots for aircraft stability and control flight testing.

The objective of this work is to develop and demonstrate a method for pilots to intuitively discover multi-axis inputs in real time that produce multi-axis flight data necessary for accurate aircraft stability and control characterization. The method, real-time software implementation, and cockpit visuals are demonstrated using a realistic F-16 nonlinear simulation. Real-time calculations, nonlinear aircraft simulation, and pilot displays for this work were implemented using a software toolbox written in MATLAB®, called System IDentification Programs for AirCraft, or SIDPAC [1,11]. The SIDPAC software toolbox was developed at NASA Langley, and has been applied successfully in a wide variety of flight-test and wind-tunnel experiments [1,7].

2. METHODS

The basic premise of the approach described in this work is that real-time modeling can be used to enable the pilot to intuitively discover effective and efficient multi-axis inputs for dynamic modeling in real time during the flight test. Although there are several methods for real-time modeling, equation-error in the frequency domain using a recursive Fourier transform implemented in a partial frequency band has been shown to be practical, efficient, and accurate in flight test applications [1,5-10]. This real-time modeling method also provides valid model parameter uncertainties, which are direct measures of the modeling accuracy that can be achieved with the flight data.

2.1. Linear Dynamic Equations

For aircraft stability and control, the dominant characteristics are in the rotational degrees of freedom described by the rotational equations of motion. Linearized aircraft equations of motion that can be used to characterize rolling, pitching, and yawing motion are [1]:

$$\dot{p} = L_\beta \Delta\beta + L_p \Delta p + L_r \Delta r + L_{\delta_a} \Delta\delta_a + L_{\delta_r} \Delta\delta_r \tag{1}$$

$$\dot{q} = M_\alpha \Delta\alpha + M_q \Delta q + M_{\delta_s} \Delta\delta_s \tag{2}$$

$$\dot{r} = N_\beta \Delta\beta + N_p \Delta p + N_r \Delta r + N_{\delta_a} \Delta\delta_a + N_{\delta_r} \Delta\delta_r \tag{3}$$

The Δ notation is used to indicate perturbation values relative to a reference flight condition, such as trimmed level flight for a specific angle of attack, aircraft configuration, and fuel state. The dimensional stability and control derivatives, such as L_β, N_r, and M_{δ_s}, are unknown model parameters to be determined from flight test data. The values of these model parameters characterize the stability and control of the aircraft at the given flight condition. Analogous linearized equations of motion can be written for the translational degrees of freedom [1].

Although the modeling can also be done using nondimensional model parameters, nonlinear equations of motion, unsteady aerodynamics, and/or nonlinear aerodynamic dependencies [1], the majority of dynamic modeling for aircraft stability and control is done using linear models such as Eqs. (1)-(3) or their nondimensional equivalents. Even if postflight data analysis and modeling determine that the modeling should be done using dynamic equations with more complexity than Eqs. (1)-(3), evaluating data information content from a flight test maneuver using the linear dynamic equations (1)-(3) is still valid, because linear model terms are important regardless of whether nonlinear terms appear in the model or not.

2.2. Equation-Error Parameter Estimation

An efficient, practical, and accurate method for determining the unknown model parameters in Eqs. (1)-(3) is called equation-error parameter estimation in the frequency domain. In this approach, the model parameter estimates are the values of the model parameters that minimize the error in each of Eqs. (1)-(3) using measured flight data. Equivalently, the model parameter estimates make the left and right sides of Eqs. (1)-(3) as nearly equal as possible, in a least squares sense. The method is called "equation-error" because the model parameters are determined by minimizing the error in each equation, analyzed individually.

The equation-error parameter estimation method will be explained first using time-domain data. Using Eq. (2) as an example, and assuming N data points were collected during a flight test maneuver, Eq. (2) can be written down N times, once for each measured data point:

$$\begin{aligned} \dot{q}(1) &= M_\alpha \Delta\alpha(1) + M_q \Delta q(1) + M_{\delta_s} \Delta\delta_s(1) \\ \dot{q}(2) &= M_\alpha \Delta\alpha(2) + M_q \Delta q(2) + M_{\delta_s} \Delta\delta_s(2) \\ &\vdots \\ \dot{q}(N) &= M_\alpha \Delta\alpha(N) + M_q \Delta q(N) + M_{\delta_s} \Delta\delta_s(N) \end{aligned} \tag{4}$$

or

$$\boldsymbol{z} = \boldsymbol{X}\boldsymbol{\theta} + \boldsymbol{\varepsilon} \tag{5}$$

where

$$\boldsymbol{z} = \begin{bmatrix} \dot{q}(1) \\ \dot{q}(2) \\ \vdots \\ \dot{q}(N) \end{bmatrix} \quad \boldsymbol{X} = \begin{bmatrix} \Delta\alpha(1) & \Delta q(1) & \Delta\delta_s(1) \\ \Delta\alpha(2) & \Delta q(2) & \Delta\delta_s(2) \\ \vdots & \vdots & \vdots \\ \Delta\alpha(N) & \Delta q(N) & \Delta\delta_s(N) \end{bmatrix} \quad \boldsymbol{\theta} = \begin{bmatrix} M_\alpha \\ M_q \\ M_{\delta_s} \end{bmatrix} \tag{6}$$

The quantity $\boldsymbol{\varepsilon}$ in Eq. (5) is a vector of equation errors. The $\boldsymbol{z}$ vector and $\boldsymbol{X}$ matrix are populated with measured data. The values of the model parameters (stability and control derivatives) M_α,

M_q, and M_{δ_s} are chosen to minimize the sum of squared equation errors in the dynamic equation for pitching motion. The quantity to be minimized is the equation-error cost function *J*:

$$J = \left(\boldsymbol{z} - \boldsymbol{X\theta}\right)^T \left(\boldsymbol{z} - \boldsymbol{X\theta}\right) = \boldsymbol{\varepsilon}^T \boldsymbol{\varepsilon} \tag{7}$$

This is equation-error parameter estimation using the dynamic equation for pitching motion. Other model parameters (stability and control derivatives) can be determined similarly using Eqs. (1) and (3).

For a flight test maneuver, there are many more equations than unknowns ($N >> 3$ in the example), and the model is linear in the unknown parameters. The optimal solution can be found using a closed-form least-squares calculation [1]:

$$\hat{\boldsymbol{\theta}} = \left(\boldsymbol{X}^T \boldsymbol{X}\right)^{-1} \boldsymbol{X}^T \boldsymbol{z} \tag{8}$$

The parameter covariance matrix is [1]:

$$\boldsymbol{\Sigma}\left(\hat{\boldsymbol{\theta}}\right) = \hat{\sigma}^2 \left(\boldsymbol{X}^T \boldsymbol{X}\right)^{-1} \equiv \left[\Sigma_{ij}\right] \tag{9}$$

where $\hat{\sigma}^2$ is the estimated equation error variance, which can be computed as

$$\hat{\sigma}^2 = \frac{\boldsymbol{\varepsilon}^T \boldsymbol{\varepsilon}}{N} \tag{10}$$

The standard error for each of the n_p estimated model parameters in the $\hat{\boldsymbol{\theta}}$ vector can be computed as the square root of the corresponding element on the diagonal of the covariance matrix,

$$s\left(\hat{\theta}_j\right) = \sqrt{\Sigma_{jj}} \qquad\qquad j = 1, 2, \ldots, n_p \tag{11}$$

2.3. Transforming Time-Domain Data into the Frequency Domain

For a data record with length *T* seconds, the analytical tool for transforming a quantity $x(t)$ (e.g., pitch rate) from the time domain to the frequency domain is the finite Fourier transform [1,10]:

$$\tilde{x}(\omega) \equiv \int_0^T x(t)\, e^{-j\omega t}\, dt \qquad\qquad \omega = 2\pi f \tag{12}$$

The Fourier transform can be computed at selected frequencies ω, which can be chosen in a partial frequency band associated with the aircraft dynamics. Zero frequency and low-frequency content are not needed to characterize aircraft stability and control, and high-frequency content composed of noise or high-frequency effects not being modeled can also be excluded. For the F-16 aircraft

used in this work, the finite Fourier transform was computed for the analysis frequencies in the frequency vector:

$$\boldsymbol{f} = \begin{bmatrix} 0.10 & 0.15 & 0.20 & \dots & 1.50 \end{bmatrix} \text{ Hz} \tag{13a}$$

or

$$\boldsymbol{\omega} = 2\pi \boldsymbol{f} = \begin{bmatrix} 0.628 & 0.942 & 1.257 & \dots & 9.425 \end{bmatrix} \text{ rad/s} \tag{13b}$$

When $x(t)$ is sampled at discrete times separated by a constant time interval Δt, the finite Fourier transform can be approximated by

$$\tilde{x}(\boldsymbol{\omega}) \approx \Delta t \sum_{i=0}^{N-1} x(i)\, e^{-j\boldsymbol{\omega} i \Delta t} \tag{14}$$

where the time length of the measured data is $T = (N-1)\Delta t$ and

$$\begin{aligned} t_i &= i\Delta t \\ x(t_i) &= x(i\Delta t) \equiv x(i) \end{aligned} \qquad i = 0, 1, 2, \dots, N-1 \tag{15}$$

Defining the summation in Eq. (14) as the discrete Fourier transform $X(\boldsymbol{\omega})$ for the analysis frequency vector $\boldsymbol{\omega}$,

$$X(\boldsymbol{\omega}) \equiv \sum_{i=0}^{N-1} x(i)\, e^{-j\boldsymbol{\omega} i \Delta t} \tag{16}$$

Combining, Eqs. (14)-(16),

$$\tilde{x}(\boldsymbol{\omega}) \approx \Delta t\, X(\boldsymbol{\omega}) \tag{17}$$

The finite Fourier transform for a time derivative $\dot{x}(t)$ can be computed by applying integration by parts with Eq. (1),

$$\begin{aligned} \int_0^T \dot{x}(t)\, e^{-j\omega t} dt &= x(T)\, e^{-j\omega T} - x(0) + j\omega \int_0^T x(t)\, e^{-j\omega t} dt \\ &= j\omega\, \tilde{x}(\omega) + x(T)\, e^{-j\omega T} - x(0) \end{aligned} \tag{18}$$

2.4. Equation-Error Parameter Estimation in the Frequency Domain

Equation-error parameter estimation in the frequency domain is analogous to equation-error parameter estimation in the time domain, discussed in section 2.2, except that the data are

transformed into the frequency domain using the finite Fourier transform. Analysis frequencies are selected in a partial frequency band that includes the aircraft dynamic response. For M selected analysis frequencies $\boldsymbol{\omega} = 2\pi \boldsymbol{f} = \begin{bmatrix} \omega_1 & \omega_2 & \dots & \omega_M \end{bmatrix}$ rad/s, the frequency-domain analogs to Eqs. (5)-(11) are [1,10]:

$$\tilde{\boldsymbol{z}} = \tilde{\boldsymbol{X}}\boldsymbol{\theta} + \tilde{\boldsymbol{\varepsilon}} \tag{19}$$

$$\tilde{\boldsymbol{z}} = \begin{bmatrix} j\omega_1 \tilde{q}(1) + q(T)\, e^{-j\omega_1 T} - q(0) \\ j\omega_2 \tilde{q}(2) + q(T)\, e^{-j\omega_2 T} - q(0) \\ \vdots \\ j\omega_M \tilde{q}(M) + q(T)\, e^{-j\omega_M T} - q(0) \end{bmatrix} \tag{20a}$$

$$\tilde{\boldsymbol{X}} = \begin{bmatrix} \Delta\tilde{\alpha}(1) & \Delta\tilde{q}(1) & \Delta\tilde{\delta}_s(1) \\ \Delta\tilde{\alpha}(2) & \Delta\tilde{q}(2) & \Delta\tilde{\delta}_s(2) \\ \vdots & \vdots & \vdots \\ \Delta\tilde{\alpha}(M) & \Delta\tilde{q}(M) & \Delta\tilde{\delta}_s(M) \end{bmatrix} \qquad \boldsymbol{\theta} = \begin{bmatrix} M_\alpha \\ M_q \\ M_{\delta_s} \end{bmatrix} \tag{20b}$$

$$J = \left(\tilde{\boldsymbol{z}} - \tilde{\boldsymbol{X}}\boldsymbol{\theta}\right)^\dagger \left(\tilde{\boldsymbol{z}} - \tilde{\boldsymbol{X}}\boldsymbol{\theta}\right) = \tilde{\boldsymbol{\varepsilon}}^\dagger \tilde{\boldsymbol{\varepsilon}} \tag{21}$$

$$\hat{\boldsymbol{\theta}} = \left[\mathrm{Re}\left(\tilde{\boldsymbol{X}}^\dagger \tilde{\boldsymbol{X}}\right)\right]^{-1} \mathrm{Re}\left(\tilde{\boldsymbol{X}}^\dagger \tilde{\boldsymbol{z}}\right) \tag{22}$$

$$\boldsymbol{\Sigma}\left(\hat{\boldsymbol{\theta}}\right) = \hat{\sigma}^2 \left[\mathrm{Re}\left(\tilde{\boldsymbol{X}}^\dagger \tilde{\boldsymbol{X}}\right)\right]^{-1} \equiv \left[\Sigma_{ij}\right] \tag{23}$$

$$\hat{\sigma}^2 = \frac{2}{T}\left[\frac{\tilde{\boldsymbol{\varepsilon}}^\dagger \tilde{\boldsymbol{\varepsilon}}}{M}\right]\left[\frac{\max(\boldsymbol{f}) - \min(\boldsymbol{f})}{f_N}\right] \qquad f_N = 1/(2\Delta t) \tag{24}$$

$$s\left(\hat{\theta}_j\right) = \sqrt{\Sigma_{jj}} \qquad j = 1, 2, \dots, n_p \tag{25}$$

2.5. Real-Time Equation-Error Parameter Estimation in the Frequency Domain

Equation-error parameter estimation in the frequency domain can be applied in real time by computing the Fourier transform recursively and applying the parameter estimation and uncertainty calculations in Eqs. (22)-(25) at selected time intervals.

The discrete Fourier transform at the ith time step, denoted by $X_i(\boldsymbol{\omega})$, can be computed recursively as follows:

$$X_i(\boldsymbol{\omega}) = X_{i-1}(\boldsymbol{\omega}) + x(i)\, e^{-j\boldsymbol{\omega} i \Delta t} \tag{26}$$

with

$$e^{-j\boldsymbol{\omega} i \Delta t} = e^{-j\boldsymbol{\omega} \Delta t} e^{-j\boldsymbol{\omega}(i-1)\Delta t} \tag{27}$$

This is called the recursive Fourier transform, and is simply calculating the discrete Fourier transform in Eq. (16) as a running sum. The update in Eq. (27) can be done efficiently using the constant vector $e^{-j\boldsymbol{\omega}\Delta t}$ for a selected analysis frequency vector $\boldsymbol{\omega}$ and constant sampling interval Δt. Applying Eq. (17) completes the calculation of the recursive Fourier transform.

Parameter estimation and uncertainty calculations in Eqs. (22)-(25) can be done at any time step, but usually are done at intervals of 0.5 s or 1 s, because significant aircraft dynamic changes will be captured using these computation intervals, except perhaps for maneuvering at very high angular rates and/or high angles of attack. Computational requirements for both the recursive Fourier transform and the parameter estimation and uncertainty calculations in the frequency domain are very low. This real-time dynamic modeling approach has been demonstrated as practical, effective, and accurate in many flight tests [1,5-12].

Time-domain perturbation quantities that feed into the recursive Fourier transform can be approximated by subtracting the initial values of the aircraft motion and control measurements at the start of the maneuver from the real-time measured data. More generally, high-pass filtering can be used for this task [1,5-12].

The equation-error variance calculation in Eq. (24) is designed for the entire maneuver, so it is not suitable for real-time calculations. Furthermore, the calculation in Eq. (24) requires equation errors computed using parameter estimation results, which means that the calculated uncertainty will depend on the parameter estimates. Instead, an independent estimate of the equation-error variance can be obtained using high-pass filtering applied to a real-time smoothed derivative of the angular rate data (i.e., angular accelerations $\dot{p}, \dot{q}, \dot{r}$) calculated in the time domain [9,12]. This is practical because only a scalar estimate of the equation-error variance is required for each dynamic equation, so that the time delay of a few sampling intervals that is required to compute smoothed derivatives of the angular rates in the time domain has no impact on the parameter uncertainty results. In this work, a 2nd-order Butterworth high-pass filter with cutoff frequency set at 3 Hz was applied to the real-time smoothed angular rate derivative data to estimate $\hat{\sigma}^2$ for use in Eq. (23). The 3 Hz cutoff frequency is above the highest analysis frequency shown in Eq. (13a). Equation-error variance estimates were computed in real time as the running average of the squared outputs from the high-pass filter applied to the smoothed angular rate derivative data. This provides an independent estimate of the equation-error variance $\hat{\sigma}^2$, so that Eq. (24) was not needed.

More details on this real-time modeling approach and applications to flight testing can be found in Refs. [1,5-12]. The real-time modeling and model uncertainty calculations were implemented in MATLAB® using tools from SIDPAC [1,11].

2.6. Advantages of Equation-Error Parameter Estimation in the Frequency Domain

Transforming the real-time measured data from the time domain into the frequency domain using analysis frequencies in a partial frequency band has important practical advantages, as follows:

1. The data are projected onto a relatively small number of sinusoidal functions with selected frequencies. This process improves accuracy by removing practically all of the wideband measurement noise, along with infrequent dropouts. The modeling is also computationally efficient with low computer memory requirements, because of the reduction in dimensionality that results from projecting the time-domain data onto a small number of sinusoidal functions.

2. Assuming that the linear model structure is adequate, the estimated parameters are unbiased with high accuracy because of the wideband noise and dropout removal, and because the analysis uses the dynamic information most relevant to the modeling [1,10,13].

3. In the frequency domain, angular acceleration ($\dot{p}, \dot{q}, \dot{r}$) data can be computed analytically from the angular rate (p, q, r) data using Eq. (18), so that measurements of the angular acceleration quantities are not needed.

4. Estimated standard errors computed in the frequency domain using Eqs. (23)-(25) are valid and accurate [1,10,13].

5. The calculations are simple, can be done efficiently in real time, and have been applied successfully in many flight tests; see [7] for a representative list.

2.7. Real-Time Flight Test Maneuver Evaluation

Uncertainties for frequency-domain equation-error parameter estimates can be computed in real time, as described in the previous section. The parameter covariance matrix $\boldsymbol{\Sigma}\left(\hat{\boldsymbol{\theta}}\right)$ in Eq. (23) can be interpreted roughly as the ratio of squared noise $\hat{\sigma}^2$ to the squared signal $\mathrm{Re}\left(\tilde{\boldsymbol{X}}^{\dagger}\tilde{\boldsymbol{X}}\right)$ for the linear dynamic modeling problem. It follows that increasing the signal-to-noise ratios for the transformed variables in the columns of $\tilde{\boldsymbol{X}}$ will decrease the standard errors for the estimated model parameters, which means more accurate stability and control derivatives and more accurate dynamic models. Furthermore, linear independence of the columns of $\tilde{\boldsymbol{X}}$ makes the matrix inverse $\left[\mathrm{Re}\left(\tilde{\boldsymbol{X}}^{\dagger}\tilde{\boldsymbol{X}}\right)\right]^{-1}$ well-conditioned, which also leads to small uncertainties for the estimated parameters. Conversely, if the columns of $\tilde{\boldsymbol{X}}$ are linearly dependent or nearly so, the resulting parameter estimates will be inaccurate and the associated uncertainties will be large [1]. The parameter covariance matrix $\boldsymbol{\Sigma}\left(\hat{\boldsymbol{\theta}}\right)$ from Eq. (23) embodies both signal-to-noise and correlations among the explanatory variables (columns of $\tilde{\boldsymbol{X}}$), so that the standard errors computed from the $\boldsymbol{\Sigma}\left(\hat{\boldsymbol{\theta}}\right)$ matrix are good metrics for the information content in the data for dynamic modeling.

The longitudinal explanatory variables α, q, and δ_s appear only in the pitching moment equation (2). However, the lateral/directional explanatory variables β, p, r, δ_a, and δ_r appear in both the rolling moment equation (1) and the yawing moment equation (3). Although $\left[\mathrm{Re}\left(\tilde{\boldsymbol{X}}^{\dagger}\tilde{\boldsymbol{X}}\right)\right]^{-1}$ will be the same for Eqs. (1) and (3), the equation-error variance $\hat{\sigma}^2$ for each equation will be different, and the estimated parameter uncertainties for each individual equation depend on the equation-error variance for that equation, cf. Eq. (23). The equation-error variance, which is different for each degree of freedom, is important for determining the explanatory variable magnitudes that must be generated during the flight test maneuver.

The real-time pilot display must clearly convey information regarding the parameter estimate uncertainties, which indicate the data information quality for dynamic modeling. To avoid cluttering the pilot display, parameter uncertainties for on-axis lateral/directional damping (L_p and N_r) and on-axis control (L_{δ_a} and N_{δ_r}) were used for the explanatory variables p, r, δ_a, and δ_r. For the remaining lateral/directional explanatory variable β, either L_β or N_β can be used with similar effectiveness. In this work, L_β was used, but this can be easily changed in the software. For the pitching moment equation, the uncertainties for model parameters M_α, M_q, and M_{δ_s} were used for the explanatory variables α, q, and δ_s.

Dynamic modeling results for the *Y* and *Z* body-axis equations of motion could also be used, if that is desired, with an easy change to the software. However, the dominant stability and control derivatives associated with these translational degrees of freedom will generally be estimated accurately if there is sufficient data information for accurately estimating the moment equation parameters. The pilot display shows only percent error bars associated with aircraft state or control variables (i.e., the explanatory variables), without the complication of showing which particular model parameter uncertainties are being used to drive the display.

The preceding development shows that pilot inputs have a significant effect on the model parameter uncertainties, and also suggests general concepts for producing informative flight data for accurate dynamic modeling. Specifically, pilot inputs that induce uncorrelated excursions in the explanatory variables that are large enough to dominate the noise will result in accurate parameter estimates (i.e., small parameter uncertainties). Some methods for doing this are moving the controls in a random and uncorrelated way, using different frequencies and applying sufficient input amplitude to excite the multi-axis aircraft dynamic response without exceeding the response limits. This piloting technique, called Uncorrelated Pilot Inputs (UPI), was developed previously and demonstrated in both simulation and in flight [3,14-15]. However, in these prior works, there were no direct indications to the pilot of how the pilot inputs affected the estimated parameter uncertainties or when the desired modeling accuracy goals were met, as in this work.

Real-time standard errors can be used as a combined indicator of both adequate signal-to-noise ratio and uncorrelated explanatory variable data. Because some model parameters have larger magnitudes than others, a good approach is to normalize the standard errors by the parameter estimate using the percent error, so that the same relative accuracy is used for all parameters. For

the *j*th estimated parameter in the estimated parameter vector $\hat{\theta}$ with length n_p, the percent error is computed as

$$\eta_j = 100\left[s\left(\hat{\theta}_j\right) \Big/ \hat{\theta}_j \right] \qquad j = 1, 2, \ldots, n_p \tag{29}$$

2.8. Flight Test Maneuver Score

The objective for the pilot is to generate multi-axis inputs that drive the percent errors for the real-time parameter estimates below selected goal values in minimum time, while keeping the aircraft response within specified boundaries. Accordingly, the scoring for each flight test maneuver was defined as:

score = (time to achieve all percent error goals) + (time outside the response boundaries) (30)

If any of the percent error goals are not achieved, then the score is set to 999. A lower score indicates a better maneuver.

The score defined in Eq. (30) is intended to encourage achieving specific percent error goals for selected important parameters in minimum time, while penalizing any time where the aircraft response exceeded limits established for the flight test maneuver. These limits could be practical flight test operational limits, or could be to maintain validity of the linear model structure (equivalently, the assumption of constant but unknown stability and control derivatives) at the flight condition for the maneuver. Other scoring methods could be used, but the scoring in Eq. (30) has direct applicability to stability and control flight test maneuver objectives and can be easily understood and internalized.

3. F-16 NONLINEAR SIMULATION

The F-16 is a single-seat, multi-role fighter with a blended wing / body and a cropped delta wing planform with leading edge sweep of 40 deg. Thrust is provided by a General Electric F110-GE-100 afterburning turbofan engine mounted in the rear fuselage. Figure 1 is a photograph of the F-16 in flight. Aircraft geometry and nominal mass properties are given in Table 1.

The F-16 nonlinear simulation has controls for throttle δ_{th}, stabilator δ_s, aileron δ_a, and rudder δ_r. Speed brake and flaps were assumed fixed at zero deflection. Nondimensional nonlinear aerodynamic force and moment coefficient data were obtained from low-speed static and dynamic (forced oscillation) wind-tunnel tests using subscale models of the F-16 [16]. The aerodynamic database applies to the F-16 flown out of ground effect with landing gear retracted and no external stores, over a wide range of angle of attack $\left(-10 \text{ deg} \le \alpha \le 45 \text{ deg}\right)$ and sideslip angle $\left(-30 \text{ deg} \le \beta \le 30 \text{ deg}\right)$.

The engine model was based on ground test data, with thrust given as a function of altitude, Mach number, and engine power level. Engine power level was computed from throttle position and throttle gearing, including first-order lag dynamics for the thrust dynamic response [16].

Figure 1. F-16 Aircraft

Credit: NASA Langley Research Center

Table 1. F-16 Properties

$\bar{c}$, ft	11.32
b , ft	30
S , ft^2	300
x_{cg} , ft	$0.25\,\bar{c}$
y_{cg} , ft	0
z_{cg} , ft	0
m , slug	637
I_x , slug-ft^2	9,496
I_y , slug-ft^2	55,814
I_z , slug-ft^2	63,100
I_{xz} , slug-ft^2	982

The F-16 nonlinear simulation was implemented completely in MATLAB®. Full nonlinear equations of motion were used, including engine gyroscopic effects. Simulation outputs were corrupted with white Gaussian noise using realistic sensor noise magnitudes. Complete details for the F-16 nonlinear simulation can be found in Ref. [1], Appendix D. The F-16 nonlinear simulation software is part of SIDPAC [1,11].

4. IMPLEMENTATION DETAILS

The real-time F-16 nonlinear simulation was implemented on a laptop computer using a Logitech 3D Pro digital joystick for the pilot inputs. Aviator Visual Design Simulator (AVDS) software was interfaced with the F-16 nonlinear simulation in MATLAB® to read pilot inputs and show real-time 3D aircraft motion [1]. The F-16 was flown with nominal mass properties and a forward center of gravity location at $0.25\,\bar{c}$ (see Table 1), so that no automatic feedback control was required. The F-16 nonlinear simulation ran at 25 Hz. The recursive Fourier transform and equation-error variance estimation were applied at every time step using the 25 Hz data from the real-time simulation. Real-time dynamic modeling calculations in Eqs. (22), (23), and (25) were done once per second.

The real-time display was built using MATLAB® plotting capabilities and tools from SIDPAC. Update rate for the data cross plots was 5 Hz and the 3D visualization of the F-16 in flight was updated at 25 Hz. Colored bar heights representing model parameter uncertainties were updated

once per second, corresponding to each real-time dynamic modeling update. All of these computations (F-16 nonlinear simulation, displays, Fourier transforms, and dynamic modeling) were done in real time on a single computing thread using an HP® EliteBook 840 G6 laptop computer. The update rates could have been higher, but those specified were found to be adequate. All pilot displays were implemented on a 24-inch desktop computer monitor.

Real-time plot animations showed a cross plot of angle of attack and sideslip angle data with limit values shown, along with control deflection cross plots and real-time parameter estimate percent error values shown as colored bars. The bars were colored green if the indicated percent error goal was achieved, and blue if not. Generally, the bar heights decrease with additional maneuvering, but not always, because the percent errors can get larger if the explanatory data become more correlated or if the aircraft response limits are exceeded.

5. DEMONSTRATION

Figure 2 is the F-16 aircraft display shown to the pilot during maneuvering. The view shown is chase pilot view with a Head-Up Display (HUD) on the lower right. This view can be changed to the pilot viewpoint inside the cockpit and several others. The green surfaces show control deflections and the yellow line length and direction indicate the air-relative velocity vector.

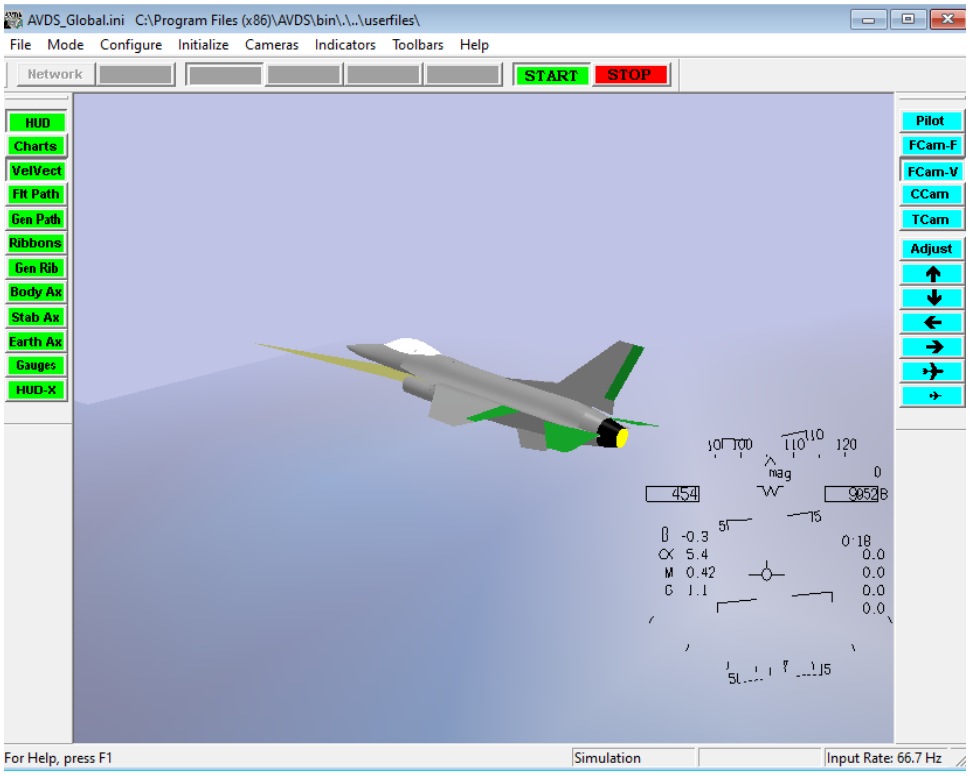

Figure 2. F-16 Aircraft Display

Figure 3 shows the pilot display for a multi-axis maneuver. The layout of the display was developed in consultation with an experienced test pilot. The colored bars at the bottom show real-time percent errors for model parameters associated with the specified explanatory variables, as described earlier. Target values were set at 5 percent, as shown by the dashed red lines. In this case, the target percent errors for some model parameters were not achieved (blue bars), whereas the target percent errors for others were achieved (green bars). Because some of the percent error goals were not achieved, the score was 999, as shown in the upper right. The plot on the upper left is a cross plot of sideslip angle and angle of attack data during the maneuver, with response limits of ±5 deg relative to the initial trim condition shown as dashed red lines. The goal is to reduce the height of the bars at the bottom to below the indicated target values as quickly as possible, while keeping the aircraft response inside the limits shown in the upper left plot. The three smaller plots on the right side are cross plots of the control deflection data: stabilator (stab), aileron (ail), and rudder (rdr). These plots indicate the decorrelation of the control deflection data in real time, which directly impacts the percent errors for the model parameters (height of the bars). In general, the control deflection cross plots should show filled-in irregular or rectangular shapes, and not lines or ellipses. For example, in Fig. 3, the control data show correlation between aileron and rudder, and sparse data coverage overall.

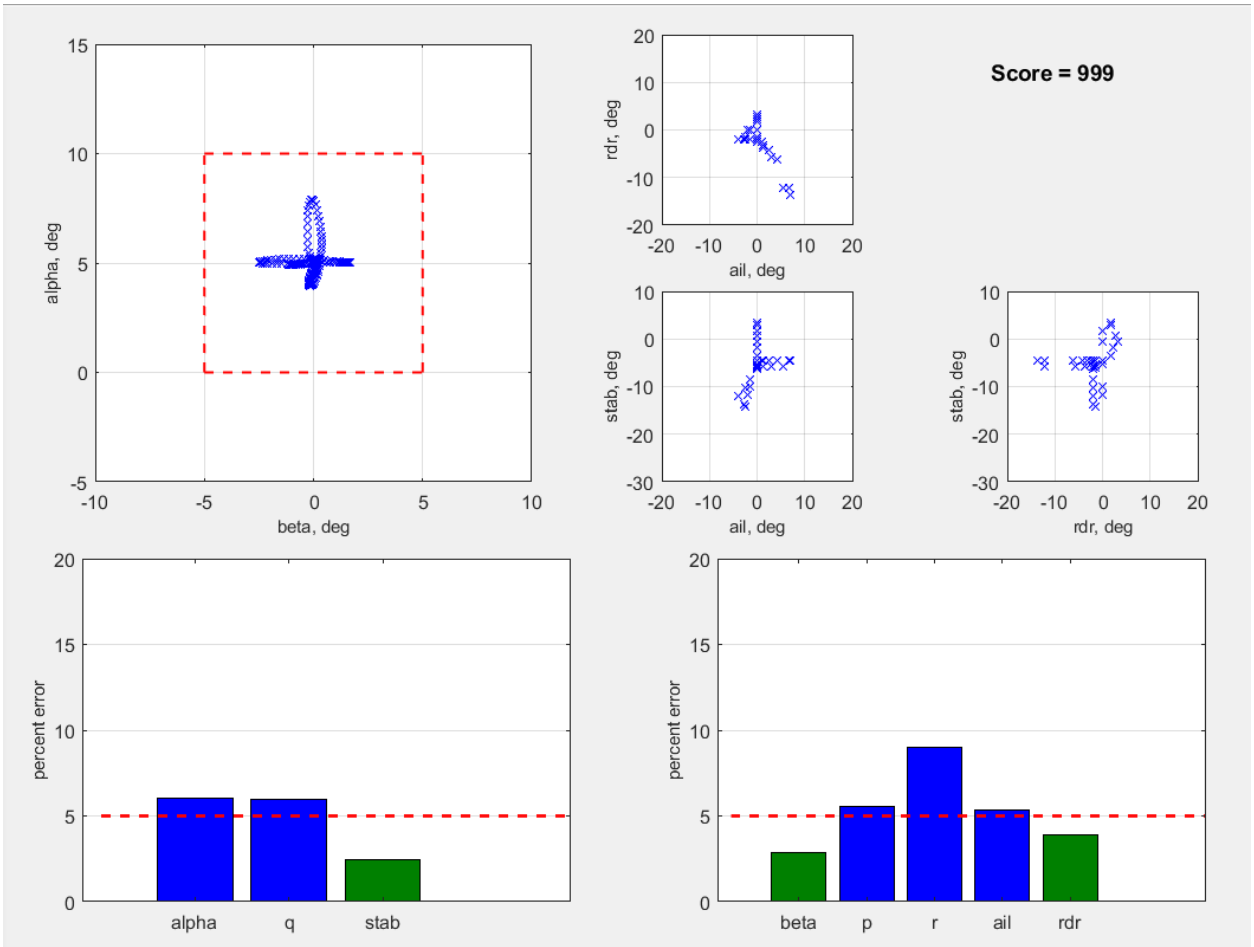

Figure 3. Pilot Display for an Inadequate Multi-Axis Maneuver

The pilot display for a successful multi-axis maneuver is shown in Fig. 4. Although the maneuver was continued for 25 s, all percent error goals were achieved in the first 11 s, without any excursions beyond the angle of attack and sideslip angle boundaries. This resulted in a score equal to 11, as shown. The pilot display showed all green bars at 11 s, indicating to the pilot that the maneuver could have been ended at that time, because sufficient data for accurate dynamic modeling had been collected. The cross plots show that all of the controls were moved in an uncorrelated fashion, with good data coverage (filled-in shapes), and angle of attack and sideslip angle response well within the response limits.

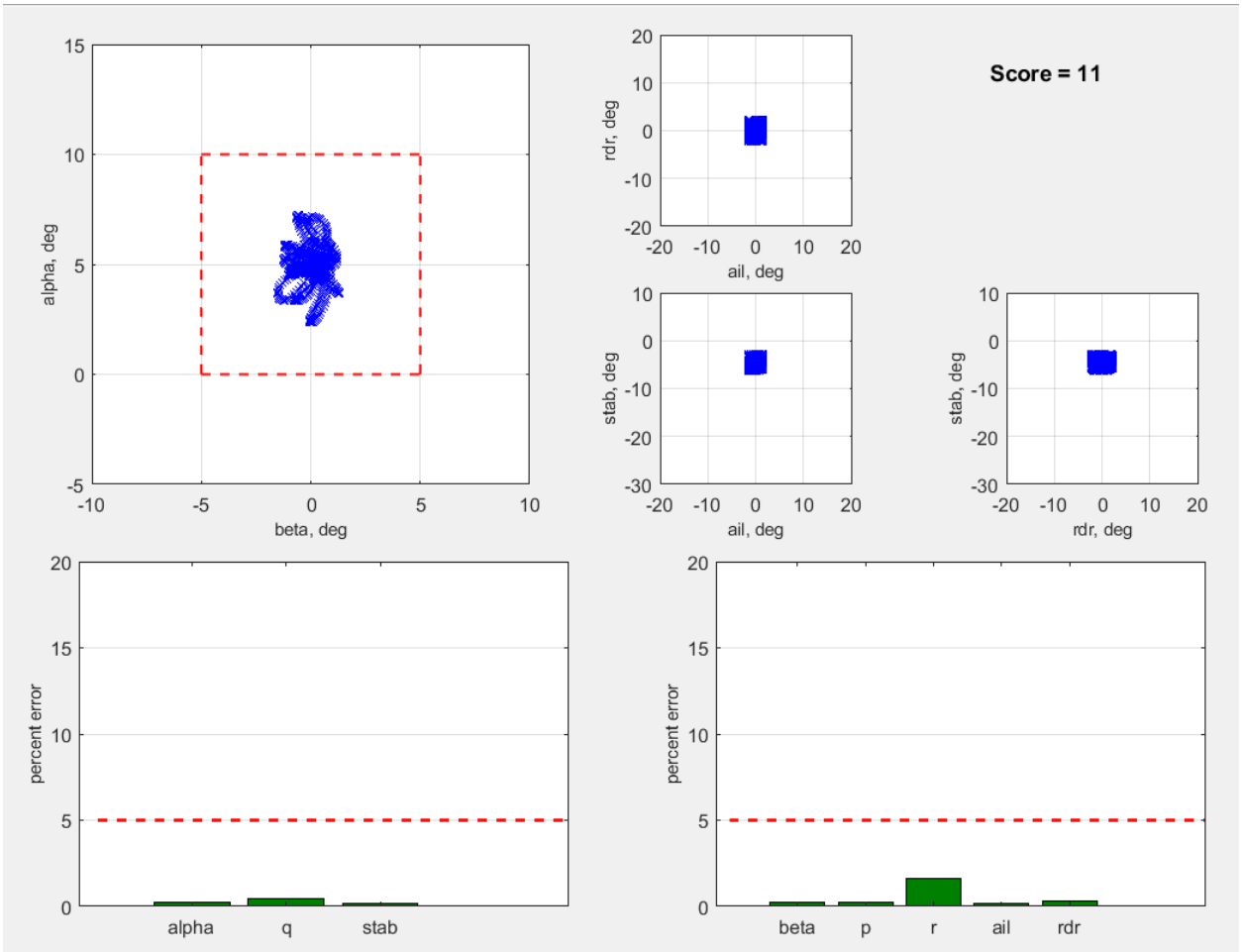

Figure 4. Pilot Display for a Successful Multi-Axis Maneuver

Figure 5 shows real-time parameter estimates for on-axis dimensional derivatives in the moment equations (1)-(3) for the pilot inputs that produced Fig. 4. Off-axis damping derivatives (such as L_r) and off-axis control derivatives (such as N_{δ_a}) were not included in Fig. 5, but the real-time estimates for these parameters exhibited similar behavior.

The dashed green lines on each plot in Fig. 5 indicate the true value of each stability or control derivative, obtained by linearizing the nonlinear F-16 simulation at the initial flight condition for

the maneuver. The blue triangle markers show the real-time parameter estimates, and the red vertical lines show the 95 percent confidence intervals $\left(\hat{\theta}_j \pm 2s\left(\hat{\theta}_j\right)\right)$, all computed in real time.

The results shown in Fig. 5 indicate that all of the parameter estimates are accurate at 11 s into the maneuver, as shown by the small red bars, as well as the stabilized real-time estimates after 11 s, and the match of the real-time parameter estimates with truth values. The plots show that the real-time parameter estimates converge quickly and accurately to the value obtained by linearizing the nonlinear F-16 simulation at the initial flight condition, and the real-time standard errors are small and representative of the true uncertainty in the real-time parameter estimates. Figure 5 also demonstrates that the pilot display in Fig. 4 was sufficient to identify when further maneuvering was not needed to improve the data information content for dynamic modeling. The information shown in Fig. 5 could also have been shown to the pilot in real time, but this would display more information to the pilot than necessary, because the pilot displays shown in Figs. 2 and 4 were sufficient for the task.

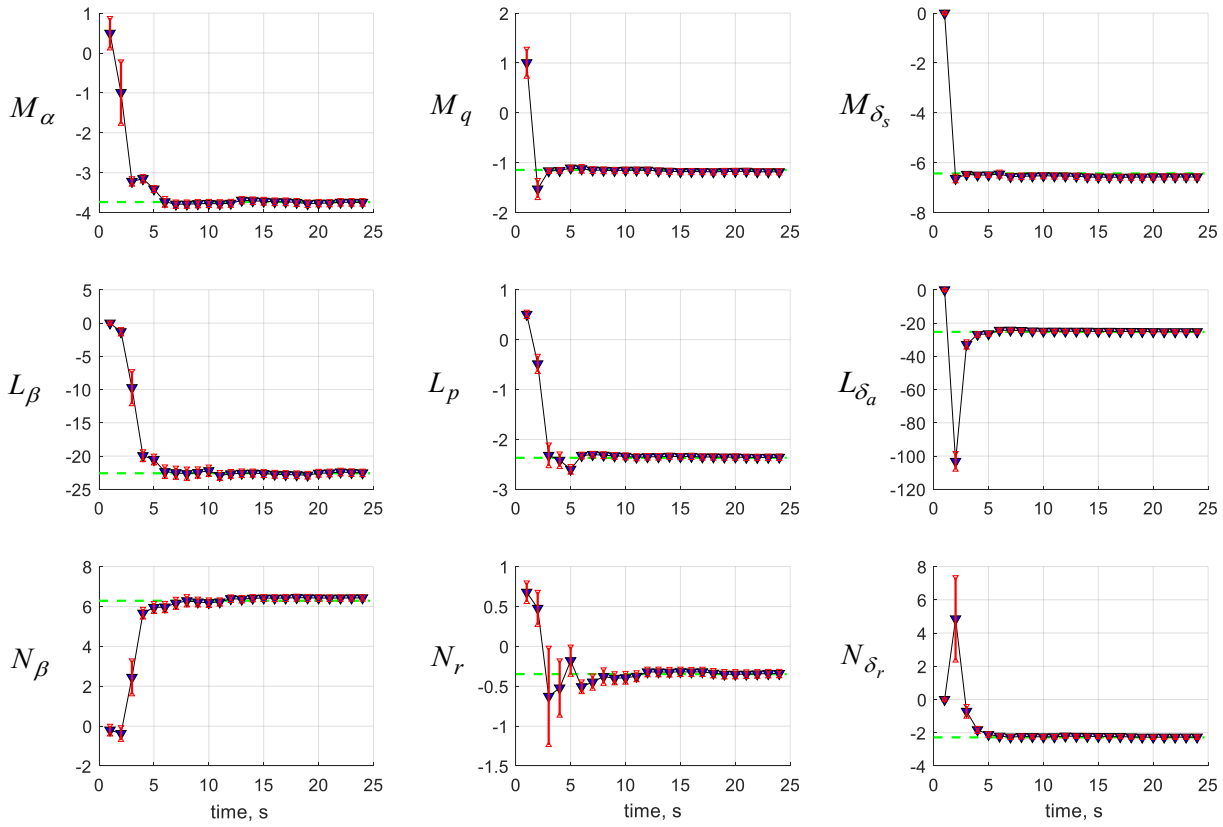

Figure 5. Real-Time Parameter Estimates for a Successful Multi-Axis Maneuver

Plots such as those shown in Fig. 5 can also be used for simulation validation and for identifying required flight updates to an existing simulation, by linearizing the simulation at the flight condition for the start of the maneuver and drawing the green dashed lines accordingly before the

flight test maneuver begins. Application of this approach in real time has been demonstrated in subscale aircraft flight testing using automated excitation inputs [17].

6. FLIGHT TEST DEMONSTRATION REQUIREMENTS

For flight test demonstration, a research aircraft instrumented for aircraft rigid-body motion (accelerometers and rate gyros), air flow angles (angle of attack and sideslip angle), center of gravity location, and control surface deflections is required. For nondimensional model parameters, airspeed, dynamic pressure, aircraft reference geometry, and aircraft mass/inertia properties would be needed. The flight testing could also be done using pilot input (stick and rudder pedal) measurements instead of control surface deflection measurements, in which case the models would be closed-loop stick-to-response models, such as Low-Order Equivalent System (LOES) flying qualities models [1,18,19]. Real-time flight data at a rate no less than 25 Hz is required. Real-time computing and real-time graphics capability in the cockpit is required, which can be implemented on a modern ruggedized laptop computer. Real-time flight data must be supplied (e.g., using Ethernet packets) to the laptop computer in the cockpit, with the laptop display screen (or a duplicate) visible to the pilot. There is no requirement for any specific test aircraft or capability, other than the real-time flight data, onboard computer, and cockpit display.

7. SUMMARY AND CONCLUSIONS

This innovation enables pilots to intuitively discover effective and efficient multi-axis inputs for accurate dynamic modeling in flight, avoiding the requirement for the pilot to implement accurate ideal input forms defined prior to flight. The advantages for flight testing are:

1. The pilot will know when to “knock it off” because sufficient informative data for accurate dynamic modeling have been collected, without requiring a call from a flight test engineer or flight test director based on preflight estimates or judgment.

2. The pilot will have real-time awareness of information deficiencies for specific model parameters or axes, so that the deficiencies can be corrected in real time during the flight test maneuver.

3. The pilot will have quantitative real-time information that can be used to improve and refine flight test inputs, with no need for intervention, training, or guidance from an analyst, flight test engineer, or flight test director.

4. New effective and efficient flight test inputs can be discovered intuitively by an expert in inducing specific aircraft dynamic responses in flight, namely, the pilot.

5. Flight test engineers no longer need to spend time and effort designing and describing specific ideal inputs for the pilot to reproduce in flight, and the training time needed for the pilot to learn how to accurately implement ideal input forms is not needed.

6. Pilots can naturally learn practical multi-axis inputs that are effective and efficient for stability and control flight testing in specific flight test situations with specific flight test aircraft, all in real time during the flight test, without any preflight analysis or preparation.

7. Successfully completing the maneuver by achieving the target parameter uncertainty goals means that the flight data collected will be sufficient for accurate dynamic modeling. No postflight analysis is needed to confirm that fact, and no repeats on another flight will be required because the maneuver went off condition or the data were insufficiently informative for accurate dynamic modeling.

The real-time system developed and demonstrated in this work would improve flight testing efficiency and effectiveness, while also providing important training for test pilots. The system can be used on any aircraft, because the dynamic modeling is done in real time specifically for the flight test aircraft, based solely on the flight data. Flight instrumentation requirements are relatively simple and typical for stability and control flight testing.

ACKNOWLEDGMENTS

Support for this research came from the NASA Aeronautics Research Mission Directorate Transformational Tools and Technologies (TTT) project and from the Dynamic Systems and Control Branch (DSCB) at NASA Langley Research Center.

REFERENCES

[1] Morelli, E.A. and Klein, V. *Aircraft System Identification - Theory and Practice*, 2nd Edition, Sunflyte Enterprises, Williamsburg, VA, Chapters 1-12, 2016.

[2] Williams, J.N., Ham, J.A., and Tischler, M.B. "Flight Test Manual, Rotorcraft Frequency Domain Flight Testing," AQTD Project No. 93–14, U.S. Army Aviation Technical Test Center, Edwards AFB, CA, September 1995.

[3] Brandon, J.M. and Morelli, E.A. "Real-Time Global Nonlinear Aerodynamic Modeling from Flight Data," *Journal of Aircraft*, vol. 53, no. 5, pp. 1261-1297, September-October 2016,

[4] Gresham, J.L., Simmons, B.M., Fahmi, J.W., Hopwood, J.W., and Woolsey, C.A. "Remote Uncorrelated Pilot Input Excitation Assessment for Unmanned Aircraft Aerodynamic Modeling," *Journal of Aircraft*, vol. 60, no. 3, pp. 955-967, May-June 2023.

[5] Morelli, E.A. "Real-Time Parameter Estimation in the Frequency Domain," *Journal of Guidance, Control, and Dynamics*, vol. 23, no. 5, pp. 812-818, September-October 2000.

[6] Morelli, E.A. and Smith, M.S. "Real-Time Dynamic Modeling – Data Information Requirements and Flight Test Results," *Journal of Aircraft*, vol. 46, no. 6, pp. 1894-1905, November-December 2009.

[7] Morelli, E.A. and Grauer, J.A. "Advances in Aircraft System Identification at NASA Langley Research Center," *Journal of Aircraft*, published online, April 2023.

[8] Morelli, E.A. "Real-Time Aerodynamic Parameter Estimation without Air Flow Angle Measurements," *Journal of Aircraft*, vol. 49, no. 4, pp. 1064-1074, July-August 2012.

[9] Morelli, E.A. "Autonomous Real-Time Global Aerodynamic Modeling in the Frequency Domain," AIAA-2020-0761, *2020 AIAA SciTech Forum*, Orlando, FL, January 2020.

[10] Morelli, E.A. and Grauer, J.A. "Practical Aspects of Frequency-Domain Approaches for Aircraft System Identification," *Journal of Aircraft*, vol. 57, no. 2, pp. 268-291, March-April 2020.

[11] https://software.nasa.gov/software/LAR-16100-1, accessed 11 January 2023.

[12] Morelli, E.A. "Practical Aspects of Real-Time Modeling for the Learn-To-Fly Concept," AIAA-2018-3309, *Atmospheric Flight Mechanics Conference, 2018 AIAA Aviation Forum*, Atlanta, GA, June 2018.

[13] Morelli, E.A. "Practical Aspects of the Equation-Error Method for Aircraft Parameter Estimation," AIAA-2006-6144, *AIAA Atmospheric Flight Mechanics Conference Proceedings*, Keystone, CO, August 2006.

[14] Brandon, J.M. and Morelli, E.A. "Nonlinear Aerodynamic Modeling From Flight Data Using Advanced Piloted Maneuvers and Fuzzy Logic," NASA/TM-2012-217778, October 2012.

[15] Morelli, E.A., Cunningham, K., and Hill, M.A. "Global Aerodynamic Modeling for Stall/Upset Recovery Training Using Efficient Piloted Flight Test Techniques," AIAA 2013-4976, *AIAA Modeling and Simulation Technologies Conference*, Boston, MA, August 2013.

[16] Nguyen, L.T., Ogburn, M.E., Gilbert, W.P., Kibler, K.S., Brown, P.W., and Deal, P.L. "Simulator Study of Stall/Post-Stall Characteristics of a Fighter Airplane With Relaxed Longitudinal Static Stability," NASA TP 1538, December 1979.

[17] Morelli, E.A. "Flight Test Maneuvers for Efficient Aerodynamic Modeling," *Journal of Aircraft*, vol. 49, no. 6, pp. 1857-1867, November-December 2012.

[18] Hodgkinson, J. "History of Low-Order Equivalent Systems for Aircraft Flying Qualities," *Journal of Guidance, Control, and Dynamics*, Vol. 28, No. 4, pp. 577-583, July-August 2005.

[19] Morelli, E.A. "Identification of Low-Order Equivalent System Models from Flight Test Data," NASA TM-2000-210117, August 2000.